

Target Tracking: Statistics of Successive Successful Target Detection in Automotive Radar Networks

Gourab Ghatak, *Member, IEEE*

Abstract—We introduce a novel metric for stochastic geometry based analysis of automotive radar networks called *target tracking probability*. Unlike the well-investigated *detection probability* (often termed as the *success or coverage probability* in stochastic geometry), the *tracking probability* characterizes the event of successive successful target detection with a sequence of radar pulses. From a theoretical standpoint, this work adds to the rich repertoire of statistical metrics in stochastic geometry-based wireless network analysis. To optimize the target tracking probability in high interference scenarios, we study a block medium access control (MAC) protocol for the automotive radars to share a common channel and recommend the optimal MAC parameter for a given vehicle and street density. Importantly, we show that the optimal MAC parameter that maximizes the detection probability may not be the one that maximizes the tracking probability. Our research reveals how the tracking event can be naturally mapped to the quality of service (QoS) requirements of latency and reliability for different vehicular technology use-cases. This can enable use-case specific adaptive selection of radar parameters for optimal target tracking.

Index Terms—Radar tracking, automotive radars, stochastic geometry, vehicular networks.

I. INTRODUCTION

Automotive radars play a critical role in modern advanced driver-assistance systems (ADAS) and autonomous driving technologies. These systems rely on accurate detection and tracking of moving objects such as vehicles, pedestrians, and other obstacles [1], [2]. In particular, radar-based target tracking ensures timely and accurate information about the target’s position, velocity, and trajectory, allowing for safer navigation and collision avoidance [3]. Given the inherent stochastic nature of the wireless environment, especially in densely populated urban scenarios, developing robust radar tracking algorithms is essential. Radar tracking is a two-step process, comprising both detection and subsequent tracking over multiple time slots with consecutive radar pulses [4]. The first step involves the successful detection of the target based on the reflected signal signal-to-interference-plus-noise ratio (SINR) [5]. In a given time slot, the target is successfully detected if the SINR exceeds a predefined threshold. Then, a target is considered successfully tracked if it is detected successfully in ν consecutive slots.

A. Motivation

The spatial statistics of the detection performance has been thoroughly investigated using tools from stochastic geometry, e.g., see [5], [6]. In particular, considering the vehicular node

locations as points of a point process, researchers have derived the probability of successful detection, the meta-distribution of the reflected signal SINR, and consequently, the mean local delay in detection. However, the statistics of consecutive successful detection events is unexplored, which we address in this work. Additionally, our model accounts for street intersections and the corresponding incoming traffic in analyzing the system performance. This is critical for developing automotive radar aided safety applications but has limited literature.

B. Related Work

In recent years, studies based on stochastic geometry have gained traction to model and analyze the statistics of automotive radar interference while addressing the variability in radar deployments, e.g., see [5]–[9]. These models are crucial for accurately evaluating radar system performance and determining the impact of interference mitigation strategies. For example, the study in [6] modeled the distribution of automotive radars using a Poisson point process (PPP) and estimated the average signal-to-interference ratio (SIR) for radar detection. Munari *et al.* [7] employed the strongest interferer approximation to assess radar detection range and false alarm rates. Additionally, the work in [8] examined radar detection probabilities by incorporating fluctuating radar cross-sections (RCS) based on Swerling-I and Chi-square models, offering more precise and intuitive outcomes compared to constant RCS models. A fine grained analysis of the impact of interference is studied in [5] where the authors derived not only the meta distribution (MD) of the SINR but also employed it to study the mean local delay in radar detection. Furthermore, they proposed an online algorithm to control the channel access by individual radars. Radar medium access control (MAC) protocols such as ALOHA and carrier sense multiple access (CSMA) have also been investigated in [10], [11]. Furthermore, asynchronous non-cooperative protocols for MAC was studied in [12]. By enhancing these models, we can improve performance evaluations, leading to the development of more optimized solutions. One of the primary advantages of using stochastic geometry frameworks is the ability to explore various spatial scenarios with significantly reduced computational resources and time compared to traditional system-level Monte Carlo simulations or real-world measurement data collection.

While these studies predominantly focus on two-lane scenarios, the authors in [13] extended the analysis to multi-lane scenarios by utilizing a marked point process model to characterize radar interference. Furthermore, more recent work has incorporated Matern Hard-Core Processes (MHCP) [14],

The author is with the Department of Electrical Engineering at the Indian Institute of Technology (IIT) Delhi, New Delhi, India 110016. Email: gghatak@ee.iitd.ac.in.

[15], which account for vehicle dimensions and the required road space, providing a more realistic interference model for automotive radar systems. However, in order to gain a more accurate view of the network, a complete two dimensional spatial model is paramount, which none of the above works address. In this regard, novel line processes have been proposed to model and study structure of streets and vehicular networks [16], [17]. In this work, we consider the Poisson line Cox process (PLCP) model for emulating the streets in order to accurately incorporate the impact of radar beamwidth (e.g., see [18] for factors impacting beamwidth selection in such networks) and the incoming traffic at intersections.

More importantly, all the above studies either focus on one shot detection, i.e., the event of successful target detection in one radar pulse transmission attempt, or characterize the mean local delay, i.e., the number of transmission attempts for first successful detection. Albeit useful, these metrics cannot estimate the performance of target tracking. To address this, we derive the distribution of run-length of successes and accordingly, characterize the statistics of successive successful detection, or tracking¹.

C. Contributions

The main contributions of this work are as follows.

- We define and derive a new metric called the tracking probability to study automotive radar networks. It characterizes the event that the ego radar is able to detect the target vehicle successfully in successive time slots. Although relevant for reliability constrained applications, this metric has not been studied yet in the context of stochastic geometry. The key technical challenge to derive this is to handle the temporal correlation in run-length of successes in a fixed time window, which is overcome using de Moivre's theorem.
- Then, we introduce a novel block ALOHA-based radar MAC protocol where active radars access the channel in a block of T consecutive slots with block probability δ . Unlike the slot-based ALOHA protocol typically assumed in automotive radar networks (e.g., see [5], [7]), the block ALOHA enables an enhanced radar tracking probability. Then we derive the detection probability of the ego radar, followed by the conditional distribution of the number of successive slots in which the reflected signal SINR exceeds a detection threshold. Furthermore, we derive the expected number of such successful tracking events in the block. As deriving the distribution of the conditional tracking probability is infeasible, we analyze its first moment, which denotes the probability of successful target tracking across all network realizations.
- Finally, we study the optimization of the tracking probability of the ego radar with respect to the channel access probability and the radar beamwidth. This enables us to derive insights into the design of adaptive cognitive

radars, specifically, how the radar parameters may be adapted in order to enable better tracking based on the street geometry, vehicle density, and use-case quality of service (QoS) requirements of latency and reliability. We show that the latency deadline of a service can be partitioned into access blocks consisting of multiple detection slots, each of which corresponds to a radar pulse width. We study the fundamental trade-off in this frame design between the block length and the number of blocks and highlight its role in maximizing successful radar tracking.

The rest of the paper is organized as follows. In Section II we describe the system model, characterize the interference set, and outline the key definitions of radar detection and radar tracking. Our main results are presented in Section III where we derive the statistics of radar tracking. Then, in Section IV, based on the derived framework, we explore QoS-Aware optimal frame design. Numerical results to highlight the salient features and insights in our framework are presented in Section V. Finally, the paper concludes in Section VI.

II. SYSTEM MODEL AND KEY DEFINITIONS

A. Street Geometry and Vehicle Locations

We consider a network of streets modeled as a homogeneous Poisson line process (PLP), $\mathcal{P} = \{L_1, L_2, \dots\}$ [20]. A line $L_i \in \mathcal{P}$ corresponds to a tuple (θ_i, r_i) , where r_i is the length of the normal to L_i from the origin and θ_i is the angle between the normal and the x -axis. The parameters $\mathbf{q}_i := (\theta_i, r_i)$ reside in the representation space $\mathcal{D} \equiv [0, 2\pi) \times (0, \infty)$. The number of parameter points, I , in any $S \subset \mathcal{D}$ follows the Poisson distribution with parameter $\lambda_L |S|$, where $|S|$ represents the Lebesgue measure of S .

The locations of the vehicles with mounted radars on the street L_i follow a one-dimensional PPP, Φ_{L_i} , with intensity λ , that represents the vehicular density. The PPP of the vehicle locations on any street is independent of the corresponding distributions on the other streets. Hence, the complete distribution of the vehicles is a homogeneous PLCP Φ , on the domain \mathcal{P} where $\Phi = \bigcup_{L_i \in \mathcal{P}} \Phi_{L_i}$. Our analysis is carried out from the perspective of an ego radar located at the origin of the two-dimensional plane. We model the ego radar as the typical point of Φ . In particular, let us define

$$\Phi^o \triangleq (\Phi \mid o \in \Phi),$$

for any point o , and note that under expectation over Φ^o , o becomes the typical point of the process Φ [21]. Since by construction, Φ is a stationary process, let us consider o to be the origin of \mathbb{R}^2 . Under Palm conditioning, a line L_0 passes through the origin almost surely, which without loss of generality, we consider to be the y -axis. The ego radar experiences interference if and only if both the ego radar and interfering radar fall into each other's radar sectors simultaneously. To model the interference from the vehicles traveling to the opposite side as the ego radar, we consider on line L_0 the location of vehicles follows a one-dimensional PPP having the same intensity as the remaining lines. Therefore, the overall spatial stochastic process of potential interfering radars,

¹ From a control systems perspective, the run-length distribution was also characterized in [19], however, there the authors did not study the same in a PLCP model and did not employ the same to study an automotive radar network, which presents its own challenges.

Φ_{P_0} , as per the Palm conditioning, is the superposition of Φ and an independent 1D PPP on line L_0 , i.e., $\Phi_{P_0} = \Phi \cup \Phi_{L_0}$.

B. Signal and Channel Model

The radars have a half-power beamwidth of Ω , and the target is assumed to be located at a distance R from the radar on the same street within the main beam of the ego radar. Let the transmit power be P and the path-loss exponent be α . The target is assumed to have a Swerling-I fluctuating radar cross-section, σ_c , with a mean of $\bar{\sigma}$ [22]. Let G_t be the gain of the transmitting antenna and A_e the effective area of the receiving antenna aperture. Then, the reflected power from the target at the ego radar is $S = \gamma \sigma_c P R^{-2\alpha}$, where $\gamma = \frac{G_t}{(4\pi)^2} A_e$. Let the coordinates of any interfering radar be denoted by $\mathbf{w} = (x, y)$, such that $x \cos \theta_i + y \sin \theta_i = r_i$ for $(\theta_i, r_i) \in \mathcal{D}_P$. The interfering signals undergo independent multi-path Rayleigh fading with parameter 1 [5]. Thus, the interference at the ego radar due to an interfering radar located at w is $\mathbf{I} = P \gamma h_{\mathbf{w}} \|\mathbf{w}\|^{-\alpha}$, where $h_{\mathbf{w}}$ is the fading power. Now, assuming that all the automotive radars share the same power and gain characteristics, the SINR at the ego radar is

$$\xi(R) = \frac{\gamma \sigma_c P R^{-2\alpha}}{N_0 + \sum_{\mathbf{w} \in \Phi_I} 4\pi \gamma P h_{\mathbf{w}} \|\mathbf{w}\|^{-\alpha}}, \quad (1)$$

where $\Phi_I \subset \Phi_{P_0}$ is the interfering set, defined and derived in the next subsection.

C. Interfering Set and Distance

The orientation of the vehicles on the street depends on the generating angle of the street and the direction of their movement. Thus, the boresight direction of any radar on the line L_i is given by the two unit vectors: \mathbf{z}_i and $-\mathbf{z}_i$, where $\mathbf{z}_i = (-\sin \theta_i, \cos \theta_i)^T$. The parameters (θ_i, r_i) , determines the direction of the radar sector on the street L_i . Any point $(p, q) \in \mathbb{R}^2$ lies in the sector if the angle made by the displacement vector between (p, q) and (x, y) and the boresight direction is larger than $\cos \Omega$. Thus, the sector of a radar located at (x, y) is either $\mathcal{R}_{(x,y)}^+$ or $\mathcal{R}_{(x,y),k}^-$ based on its direction, mathematically defined below.

Definition 1. [17] *The radar sector of a vehicle located at $(x, y) \in \Phi_{P_0}$ for boresight direction \mathbf{z}_i is*

$$\begin{aligned} \mathcal{R}_{(x,y)}^+ &= \left\{ (p, q) \in \mathbb{R}^2 : \frac{((p, q) - (x, y)) \cdot \mathbf{z}_i}{\|(p, q) - (x, y)\|} > \cos \Omega, \right. \\ &\quad \left. \|(p, q) - (x, y)\| \leq R \right\} \\ &= \left\{ (p, q) \in \mathbb{R}^2 : \frac{\cos \theta_i (q - y) - \sin \theta_i (p - x)}{\sqrt{(p-x)^2 + (q-y)^2}} > \cos \Omega, \right. \\ &\quad \left. \sqrt{(p-x)^2 + (q-y)^2} \leq R \right\}. \end{aligned}$$

And for boresight direction $-\mathbf{z}_i$,

$$\begin{aligned} \mathcal{R}_{(x,y)}^- &= \\ &\left\{ (p, q) \in \mathbb{R}^2 : \frac{\sin \theta_i (p - x) - \cos \theta_i (q - y)}{\sqrt{(p-x)^2 + (q-y)^2}} > \cos \Omega, \right. \\ &\quad \left. ; \sqrt{(p-x)^2 + (q-y)^2} \leq R \right\}. \end{aligned}$$

The ego radar sector corresponds to the line $(\theta_i, r_i) = (0, 0)$ and the location $(x, y) = (0, 0)$. If ego radar is located within the radar sector of the radar present at (x, y) i.e., $\mathbf{1} \left((0, r) \in \mathcal{R}_{(x,y)}^+ \right) + \mathbf{1} \left((0, r) \in \mathcal{R}_{(x,y)}^- \right)$ evaluates to one, and simultaneously the automotive radar located at (x, y) is located in the interior region of ego radar sector i.e., $\mathbf{1} \left((x, y) \in \mathcal{R}_{(0,r)}^+ \right) + \mathbf{1} \left((x, y) \in \mathcal{R}_{(0,r)}^- \right)$ evaluates to one, then radar at (x, y) will be an element of Φ_I . From the perspective of the ego radar, the following result characterizes the location of the interfering radars on each street L_i .

Lemma 1. *For line L characterized by the PLP point (r, θ) where $0 < \theta \leq \frac{\pi}{2}$, that intersects L_0 at a distance d from the ego radar, the minimum (a) and the maximum (b) distances of the interfering radars from the point of intersection are*

$$\begin{aligned} a &= \frac{d \sin(\theta - \Omega/2)}{\sin \Omega/2} \\ b &= \frac{\sin \Omega/2}{d \sin(\theta - \Omega/2)}. \end{aligned}$$

Proof: Please see Appendix A. ■

With this characterization we note that $\Phi_I = \cup_{i \in \mathcal{P}} (\Phi_{P_0} \cap (a_i, b_i) \mathbf{z}_i)$. It must be noted that here we have made an abuse of notation by referring to the PLCP as a subset of the PLP thus allowing for the intersection of the elements of the two sets. This is well-defined iff the PLP itself is defined as a subset of \mathbb{R}^2 and not merely a set of lines. However, this notation allows us to simplify the expressions and does not cause any deviation from the correctness of the results. Based on this interfering set, we study the tracking performance of a radar access protocol defined next.

D. Radar MAC Protocol

In dense vehicular networks, in particular where the radar and communication bands are shared, frequent radar signals may degrade the overall detection as well as the communication performance. For this, we propose a tunable block ALOHA protocol for shared radar channel access. Let the time frames be divided into blocks of T slots each. In each block, only a subset of the vehicles are allowed to activate their radars. The activation set follows the classical ALOHA protocol with parameter $\delta \in [0, 1]$. Thus, each vehicle in Φ_P operates in a block with probability δ . Within the block, it attempts to detect the target in each of the T slots. We present our analysis from the perspective of a single such block in which the ego radar is active. Later, we discuss the intricacies of designing the block length in Section IV. Here we define

the key metrics that we statistically characterize in the next section.

Definition 2 (Successful target detection). *We define the target to be successfully detected in a slot if $\xi \geq \gamma$ for some threshold γ .*

Let L denote the maximum run length of detection successes in a block for the ego radar, i.e., it is the largest number $L \in [0, T]$, such that the ego radar experiences L consecutive successful target detection in consecutive. We call L as the tracking length, which is a random variable.

Definition 3 (Successful target tracking). *We define the target to be successfully tracked in a block of length T slots if the ego-radar successfully detects the target in ν consecutive slots, i.e., the event $L \geq \nu$, for some $\nu \leq T$.*

III. STATISTICS OF RADAR TRACKING

In order to characterize the radar tracking, first we derive the probability of a successful detection event in one slot given that the ego radar is active in the block.

Lemma 2. *The conditional probability of successful target detection in a slot by the ego radar given that it is active in the block is given by*

$$P_d = \exp\left(\frac{-\gamma}{\xi_0 R^{-2\alpha}}\right) \left(\prod_{\mathbf{w} \in \phi'} \frac{1}{1 + \frac{\gamma d_{\mathbf{w}}^\alpha}{R^{-2\alpha}}}\right), \quad (2)$$

where $\xi_0 = \frac{P}{N_0}$ is the transmit signal-to-noise ratio (SNR) and ϕ' is an instance of Φ' which is a thinned version of Φ_I where the PPP on each line has an intensity $\delta\lambda$.

Proof: Please see Appendix B. ■

It is worth to note that due to the conditioning on Φ , P_d is a random variable defined on a suitable sigma field where the counting measure Φ is defined. Indeed, conditioned on Φ , the above success event is an independent random variable across the time slots of a block when the ego radar is active. It is precisely this random variable that we characterize in this work. The probability P_d changes across blocks as the set of active radars changes.

Remark 1. *The conditional success probability in (2) is different from that derived in [5], [10], [11]. In particular, the above works consider random access in each slot and hence, there the transmission state of each radar needs to be averaged out with respect to the ALOHA parameter. However, in our case, once the transmission states of the radars are determined at the beginning of the block, the same remains fixed throughout all the slots of the block. Hence, the impact of the ALOHA only appears in the set over which the product of the point functions is evaluated in (2).*

We characterize the conditional probability of successful target tracking based on the above result.

Remark 2. *Leveraging de Moivre's solution [23, Section 22.6], the conditional complementary cumulative density func-*

tion (CCDF) $F_L(\nu) = \mathbb{P}(L \geq \nu \mid \Phi)$ of L as a function of P_d is

$$F_L(\nu) = \sum_{l=1}^{\lfloor \frac{T+1}{\nu+1} \rfloor} (-1)^{l+1} \left(P_d + \frac{T - l\nu + 1}{l} (1 - P_d) \right) \times \binom{T - l\nu}{l - 1} P_d^{l\nu} (1 - P_d)^{l-1}. \quad (3)$$

The above result establishes the probability of successful target tracking for a given realization ϕ of Φ and a given access states for the active radars. Next, we look at the target tracking performance averaged over the network realization using the moments of conditional success probability.

Lemma 3. *Given that the ego radar is active in a block, the moments of conditional success probability P_d of the typical controller at a given time t within the block is given by*

$$\begin{aligned} \zeta(l) &= \mathbb{E}[P_d^l] \\ &= \exp\left(-\lambda\delta \int_0^\infty 1 - \mathcal{T}_z^l dz\right) \cdot \exp\left(-2\lambda_L \int_0^{2\pi} \int_0^\infty 1 - \exp\left(-\delta\lambda \int_{a_i}^{b_i} 1 - \mathcal{T}_{z,x}^l dz\right) dx d\theta\right), \end{aligned} \quad (4)$$

where $\mathcal{T}_z = \left(\frac{R^{-2\alpha}}{R^{-2\alpha} + \gamma z^{-\alpha}}\right)$, $\mathcal{T}_{z,x} = \frac{R^{-2\alpha}}{R^{-2\alpha} + \gamma w(x,z,\theta)^{-\alpha}}$ and $w(x,z,\theta) = x^2 + z^2 + 2xz \cos \theta$.

Proof: Please see Appendix C. ■

The above result immediately leads to some interesting insights about the expected number of bursts that exceed the desired length and the expected burst length averaged across all network instances.

Theorem 1. *The expected number of successful tracking events across all network instances is $(T - \nu + 1)\zeta(\nu)$, and the expected tracking length is $\mathbb{E}[L] = \sum_{l=1}^T \zeta(l) - T\zeta(T + 1)$.*

Proof: Please see Appendix D. ■

Corollary 1. *For $T = \infty$ and the same arguments as that of the proof of Theorem 1, the expected tracking length is the sum of the moments $\sum_{l=1}^\infty \zeta(l)$.*

Further, we define the MD of the burst length L as the distribution of $F_L(\nu)$, i.e.,

$$\mathcal{M}_B(\nu, \beta) = \mathbb{P}(F_L(\nu) \geq \beta),$$

where $F_L(\nu) = \mathbb{P}(L \geq \nu \mid \Phi)$ is the conditional CCDF of L as defined in (3). In other words, $\mathcal{M}(\nu, \beta)$ represents the fraction of radars in the network that experience a successful successive detection of at least ν slots in a sequence of T slots in at least β fraction of the network realization. Unlike the MD of the SINR in wireless networks, we observe that the MD of the tracking length is challenging to derive even indirectly via its moments. However, if all the radars have the same desired tracking length ν , the first moment of the distribution is given by $\mathbb{E}[F_L(\nu)]$ in Theorem 2 below.

Theorem 2. *Given that the ego radar transmits, the first moment of the conditional CCDF of the tracking length, or*

the tracking probability is

$$P_t = \mathbb{E}[F_L(\nu)] = \sum_{l=1}^{\lfloor \frac{T+1}{\nu+1} \rfloor} (-1)^{l+1} \binom{T-l\nu}{l-1} \\ \times \left(\sum_{\ell=0}^{l-1} \binom{l-1}{\ell} (-1)^\ell \zeta(l\nu+1+\ell) \right) \\ + \frac{T-l\nu+1}{l} \sum_{\ell=0}^l \binom{l}{\ell} (-1)^\ell \zeta(l\nu+\ell). \quad (5)$$

Proof: From (3), the expected value of $F_L(\nu)$ is

$$\mathbb{E}[F_L(\nu)] = \sum_{l=1}^{\lfloor \frac{T+1}{\nu+1} \rfloor} (-1)^{l+1} \binom{T-l\nu}{l-1} \\ \times \mathbb{E} \left[P_d^{\nu+1} (1-P_d)^{l-1} + \frac{T-l\nu+1}{l} P_d^{\nu} (1-P_d)^l \right].$$

Using the Binomial expansion $(1-P_d)^l = \sum_{\ell=0}^l \binom{l}{\ell} (-1)^\ell P_d^\ell$ and some trivial simplification, we arrive at the result. ■

IV. QOS-AWARE OPTIMAL FRAME DESIGN

In this section, we use the above framework for the design of the transmit frames and the selection of optimal access probability from the perspective of specific automotive use-cases. Let us define T_L as the latency requirement specified by the use-case. As an example, low-latency applications such as lane change assistance and automatic emergency braking (AEB) may employ a T_L of the order of 1 ms (note that this not the end-to-end latency, but only the latency over the radio link). On the contrary, use-cases that have less stringent latency requirements such as blind spot detection, park assist etc have T_L of the order of 10 ms. Some indicative latency requirements are outlined in Table I. Furthermore, we introduce a reliability measure based on the parameter ν . In particular, a larger value of ν corresponds to a higher reliability requirement from the service. For the tracking service to be rendered successful, let us assume that within the latency deadline, the use-case necessitates at least one successful tracking event, i.e., the ego radar experiences at least one burst of ν consecutive successes within a deadline of T_L .

As per the radar MAC introduced in this work, let the duration T_L be divided into N access blocks, wherein, each radar competes for access in each block. Recall that each block is further divided into T slots, each corresponds to one pulse width W of the radar. Naturally, the choice of N (and consequently, T) depends on the required ν of tracking, which in turn, depends on the use-case. In particular, we have

$$N = \left\lfloor \frac{T_L}{TW} \right\rfloor, \quad (6)$$

where T must be necessarily larger than ν . For a specific use case, the probability that the target is successfully tracked in at least one of the tracking attempts within the latency deadline is thus $(1 - (1 - \delta)^N) P_t$. This naturally incorporates the spatial correlation of each network realization since for a fixed δ , $\mathbb{E}[(1 - (1 - \delta)^N) \mathbb{P}(L \geq \nu | \Phi)] = (1 - (1 - \delta)^N) \mathbb{E}[F_L(\nu)]$.

A natural trade off arises - fewer blocks results in a lower access chance for individual radars for activation during T_L , i.e., a lower value of $(1 - (1 - \delta)^N)$. However, it results in a larger T in each block which enables a higher probability that the tracking length of an active radar exceeds ν , i.e., a larger P_t . Two extreme cases are of special interest - one where the entire latency period is allotted to all the radars for access, i.e., we set $TW = T_L$. The other case is to set $T = \nu$, i.e., the block length is exactly equal to the reliability requirement.

An optimal frame design along with an optimal access policy needs cognitive information about the number of competing radars. It is mathematically formulated as follows.

$$\max_{\delta, N} (1 - (1 - \delta)^N) P_t \\ \text{st. } P_t \text{ as in (5)} \\ N = \left\lfloor \frac{T_L}{TW} \right\rfloor \leq \left\lfloor \frac{T_L}{\nu W} \right\rfloor \\ 0 \leq \delta \leq 1$$

The above formulation is a mixed integer non-linear program, where the parameters λ and λ_L may not be known to the ego-radar. This necessitates the development of data-driven algorithms for optimizing the tracking performance, which is currently out of scope of this paper where our focus is mainly on the statistical characterization. Nevertheless, we make a couple of critical remarks.

Remark 3. *The case $\delta = 1$ corresponds to full interference (no MAC protocol). In this case, regardless of the value of ν , the optimal solution is to select $N = 1$ and accordingly $TW = T_L$.*

Indeed, for the full interference scenario, any other choice of N simple reduces the block length without improving the tracking probability. The case $\nu = 1$ corresponds to maximizing the detection probability, i.e., at least one successful detection in the block. We will see in the next section that the optimal δ decreases with an increase in λ and λ_L due to an increase in interference. Hence, for a given block size, block length, and ν , the optimal δ can be read out from an appropriate look-up table.

Remark 4. *The optimization over N is simple since the search space is finite. Starting from $N = 1$, each step increase in N reduces the block length by half. Thus, the search space for N is $[1, \log_2(T_L/W)]$.*

In case of a finite set of access probabilities, as is the case in most practical deployments, the optimal pair of N and δ can thus be stored for given λ and λ_L .

V. NUMERICAL RESULTS AND DISCUSSION

In this section we discuss the salient features of the network with the help of some numerical results. The radar parameters used for the numerical results are taken from [24]. Specifically, $P = 10$ dBm, $\bar{\sigma} = 30$ dBsm, $\alpha = 2$, $G_t = 10$ dBi, $f_c = 76.5$ GHz, and $N_0 = -174$ dBm/Hz. Unless otherwise stated, we assume $R = 15$ m. The street and vehicle densities are from [17] where the authors have reported real-world data on the same.

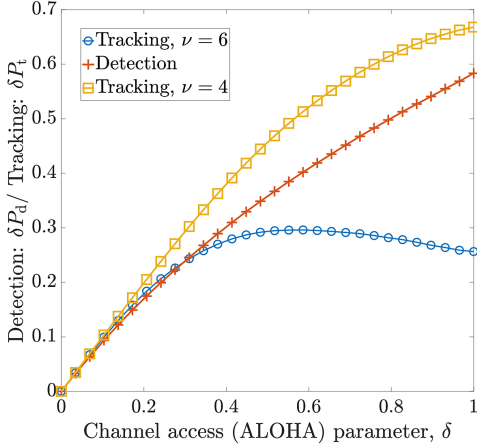


Fig. 1. Comparison of detection and tracking performance with respect to the ALOHA parameter. Here $\lambda = 5e - 2 \text{ m}^{-1}$, $T = 20$ slots, $\nu = 6$, and $\lambda_L = 5e - 4 \text{ m}^{-1}$.

A. Detection vs tracking performance

First, we discuss the key insights that our analysis provides as compared to the existing works on stochastic geometry based automotive radar analysis. In Fig. 1 we plot the radar detection probability in one slot multiplied with the channel access probability, i.e., δP_d and compare it with the tracking probability in one block multiplied with the block access probability, i.e., δP_t . Based on the reliability requirement, ν , the tracking probability may vary drastically. A low ν enables a higher tolerance of interference. In particular, we see that for $\nu = 4$, the framework recommends an optimal $\delta = 1$, as even in the full interference regime, the event $L \geq \nu$ is achieved with the highest probability. On the contrary, a more stringent reliability requirement, e.g., $\nu = 6$ necessarily requires access control - here the optimal δ is near 0.5. In other words, even though half of the radars do not access the channel on an average, the resultant lower interference results in an improved tracking probability. We further note that $\nu = 4$ has an improved tracking probability as compared to the detection probability. For explaining this, is worth to recall that as per the block MAC protocol introduced in this paper, once a radar is active in a block, it transmits in all the slots of the block. This is contrary to the detection event where the radar competes for access in all the slots of the block. Hence, for a lower value of ν , a successful channel access in a block may be sufficient for a successful tracking event, especially in the low δ (low interference) regime.

B. Impact of Street and Vehicle density

Fig. 2 shows that the street geometry and the vehicle density influences not only the optimal channel access probability

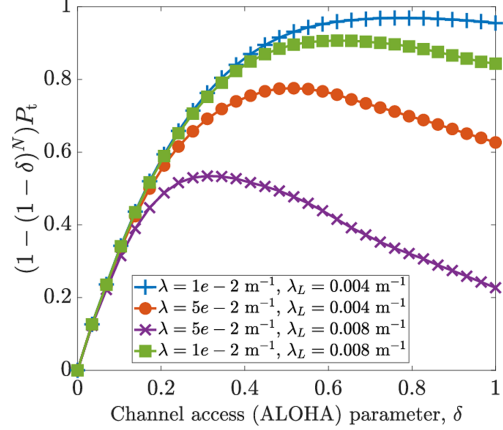


Fig. 2. Impact of the street and vehicle density on the tracking performance. Here $T = 20$ slots, $K = 4$, and $\nu = 6$.

but also dictates the trends of the tracking performance $(1 - (1 - \delta)^N P_t)$. For dense streets, e.g., in the city center, an increase in δ leads to a higher increase in the interference as compared to scenarios with fewer streets. Accordingly, dense street scenarios necessitate stringent access control, facilitated by a lower value of δ . A higher vehicle density reduces the tracking probability of the ego radar. This also necessitates the employment of a carefully designed MAC policy. This is illustrated in Fig. 3 where we see that the optimal δ decreases with an increase in either λ or λ_L . Although the optimal δ for low λ is 1 for both $\lambda_L = 0.004 \text{ m}^{-1}$ and $\lambda_L = 0.006 \text{ m}^{-1}$, the optimal δ decreases more rapidly for a higher value of λ_L . Furthermore, Fig. 4 shows the trends in the conditional expectation of the number of successful bursts of 8 or more successive successful detection events in a block of length 20. The condition is on the event that the ego-radar accesses the channel in the block under consideration. Note that the maximum value of the conditional expectation in this case is 10. Higher the ALOHA parameter, lower are the number of successful bursts experienced by the ego-radar. The number of successful bursts required depend on the use-case QoS requirement and must be carefully studied. This is more crucial since the analysis in Fig. 4 considers overlapping bursts, which may or may not be suited for a given service. This is further discussed below.

C. Impact of Use-Case QoS Requirements

Fig. 5 shows the impact of the latency deadline T_L and the reliability requirement modeled as the number of consecutive slots of detection ν . Specifically, we study two services - lane change assist [27] with a typical latency requirement of the order of 10 ms, and automatic emergency braking [28] with a

Use Case	Latency T_L	Reliability, ν	δ^*
Adaptive Cruise Control (ACC)	≤ 100 ms	10	1
Automatic Emergency Braking (AEB)	≤ 50 ms	15	0.8
Blind Spot Detection (BSD)	≤ 200 ms	5	1
Lane Change Assistance	≤ 100 ms	15	0.4
Pedestrian Detection	≤ 50 ms	15	0.8
Park Assist	≤ 100 ms	1	1
Intersection Management	≤ 50 ms	15	0.8

TABLE I: Use cases and corresponding latency and reliability requirement derived from [25] and [26]. However, note that the latency requirement mentioned here is not end-to-end latency, but the latency over the radio link. The figures are indicative and real values are system dependent. The optimal channel access probability is calculated against each use-case. We assume $\lambda = 5e - 2 \text{ m}^{-1}$ and a beamwidth of 10 degrees.

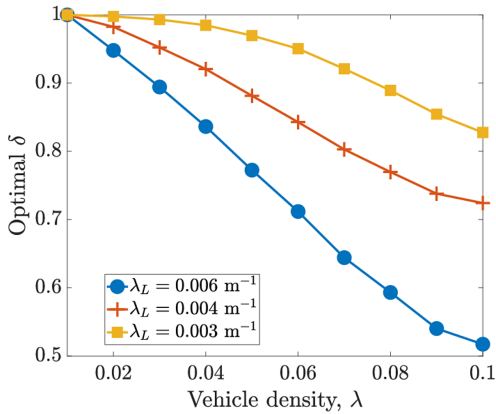


Fig. 3. Optimal δ for different vehicle and street density. Here we fix $T = 25$ and $N = 4$.

typical latency of 1-3 ms. Note that these latency requirements from the radio link and not end-to-end latency. Furthermore, let us specify two reliability requirements: $\nu = 8$ and $\nu = 12$. For the results of this figure, we fix the number of slots per block as $T = 20$. We assume a pulse width of $200 \mu\text{s}$. This results in $K = 50$ blocks for the lane change assist use-case and $k = 15$ blocks for the automatic emergency braking use-case. Recall that for the service to be rendered successful, the ego radar needs at least one successful tracking event. Due the larger number of blocks to compete in for access, the success probability is higher for the lane change assist use-case as compared to the automatic emergency braking use-case. Interestingly, for higher reliability requirement ($\nu = 12$), not only the success probability is lower, but also the optimal δ is higher. In Table I we show example use-cases with corresponding latency and reliability requirements. Accordingly, the optimal channel access probability is demonstrated. The optimization of δ is not straightforward due to the two

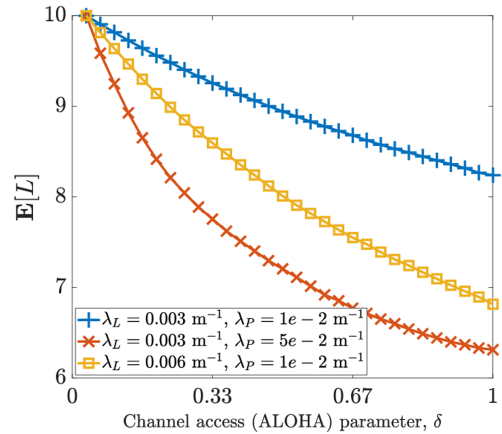


Fig. 4. Expected number of bursts with a length $\geq \nu = 8$ for $T = 20$ for different λ_P and λ_L . Here we have assumed

competing phenomenon of interference and channel access. in this regard, we discuss the considerations for the optimal frame design next.

D. Optimal Frame Design

As discussed in the previous section, a larger value of N results in smaller block lengths. This facilitates a larger number of attempts for the ego-radar to access transmission, but puts a more stringent demand on the tracking event. In this section, we investigate the impact of the beamwidth on optimal frame design. For a beamwidth of 10 degrees, Fig. 6 shows that for lower values of δ , a higher value of N results in an improved tracking performance. Indeed, when fewer interferers are active (lower δ), a limited number of access opportunities for the ego radar can result in a successful target tracking. However, in case of high interference (higher δ), a larger number of access attempts are necessary. As noted in Remark 3, for $\delta = 1$, higher the value of N , lower is the

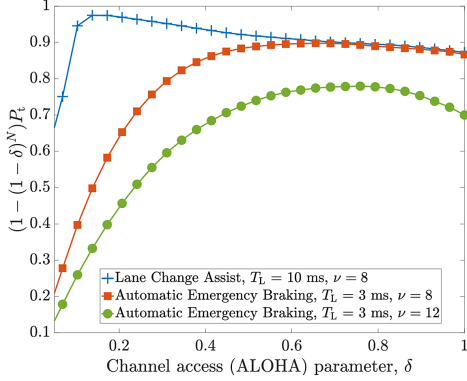


Fig. 5. Impact of the use-case QoS requirements on the tracking performance. Here we fix $T = 20$ slots.

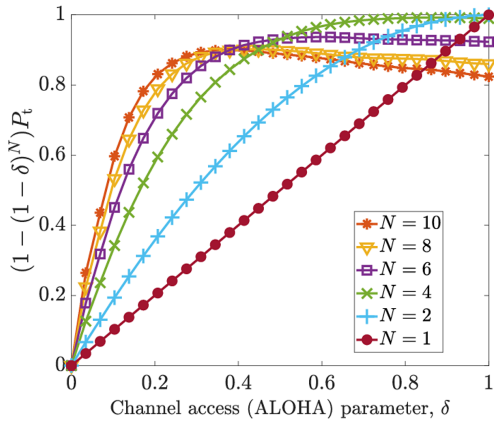


Fig. 6. Impact of the frame design policy on the tracking performance. Here we use real data fitting of New Delhi city to extract the PLCP parameter $\lambda_L = 0.004 \text{ m}^{-1}$ (see [17] for details) and use a vehicle density of $\lambda = 5e - 2 \text{ m}^{-1}$ and $\Omega = 10$ degrees.

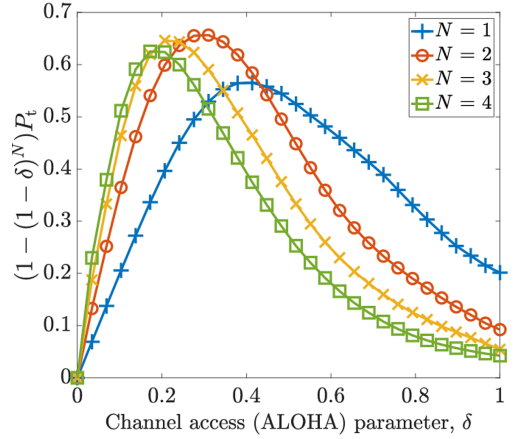


Fig. 7. Impact of the frame design policy on the tracking performance for a wide beamwidth: $\Omega = 50$ degrees.

tracking success. For this particular case, we see that $N = 1$ and $\delta = 1$ is optimal (in terms of $(1 - (1 - \delta)^N)P_t$).

In case of a higher beamwidth, e.g., $\Omega = 50$ degrees, Fig. 7 shows that $N = 1$ may not be optimal. A larger Ω corresponds to a larger number of interfering radars appearing within the radar sector of the ego-radar, albeit with a lower radiated power. In this case, we see that $N = 2$ results in a higher tracking performance when δ is optimally chosen (0.3) in this case. Similar to the previous case, the optimal δ is lower for a larger value of N . This follows naturally since a higher N results in a shorter blocks size, which necessitates a more stringent access control to limit the interference.

VI. CONCLUSION

We introduced and characterized radar tracking probability, which is a novel metric to study automotive radar networks using stochastic geometry. Although the radar detection has been studied at length in literature, the statistics of successive successful detection has not been explored before. Using de Moivre's theorem, we derived the probability that an active radar experiences a success burst of length ν or more in a block of T slots. The latency and reliability QoS requirements of automotive use-cases can be mapped to the parameters ν and T of our framework. We considered a block ALOHA based MAC protocol to control the set of active radars and demonstrated that optimal selection of block length is non-trivial. A larger block length improves the tracking performance of active radars in that block, but it results in a fewer radars getting activated within the radar deadline. For a given choice of block length, the optimal channel access parameter can be obtained via algorithms such as hill-climbing due to the unimodal nature of the tracking success with respect to the access parameter. In

where P_d^v is given by (2). So, from Lemma 3, the expected number of bursts averaged over the point process is

$$\begin{aligned}\mathbb{E}[B(k)] &= \mathbb{E}[\mathbb{E}[B|\Phi]] = (T - L + 1)\mathbb{E}[P_d^L] \\ &= (T - L + 1)\zeta(L).\end{aligned}$$

Similarly, to obtain the expected tracking length \bar{L} , we derive

$$\begin{aligned}\mathbb{E}[L] &= \mathbb{E}\left[\sum_{l=0}^T lP_d^l(1 - P_d)\right] \\ &= \mathbb{E}\left[\frac{TP_d^{T+2} - TP_d^{T+1} - P_d^{T+1} + P_d}{1 - P_d}\right] \\ &= \mathbb{E}\left[\frac{P_d - P_d^{T+1}}{1 - P_d} - TP_d^{T+1}\right] = \mathbb{E}\left[\sum_{l=1}^T P_d^l - TP_d^{T+1}\right].\end{aligned}$$

Combining the last step with Lemma 3, we obtain the expected burst length \bar{L} .

REFERENCES

- [1] X. Dong *et al.*, "Probabilistic oriented object detection in automotive radar," in *Proceedings of the IEEE/CVF Conference on Computer Vision and Pattern Recognition Workshops*, 2020, pp. 102–103.
- [2] S. M. Patole *et al.*, "Automotive radars: A review of signal processing techniques," *IEEE Signal Processing Magazine*, vol. 34, no. 2, pp. 22–35, 2017.
- [3] X. Cao *et al.*, "Automotive radar-based vehicle tracking using data-region association," *IEEE Transactions on Intelligent Transportation Systems*, vol. 23, no. 7, pp. 8997–9010, 2021.
- [4] D. D. Howard and M. Skolnik, "Tracking radar," *Radar handbook*, pp. 18–43, 1990.
- [5] G. Ghatak *et al.*, "Radar detection in vehicular networks: Fine-grained analysis and optimal channel access," *IEEE Transactions on Vehicular Technology*, vol. 71, no. 6, pp. 6671–6681, 2022.
- [6] A. Al-Hourani *et al.*, "Stochastic geometry methods for modeling automotive radar interference," *IEEE Transactions on Intelligent Transportation Systems*, vol. 19, no. 2, pp. 333–344, 2017.
- [7] A. Munari *et al.*, "Stochastic geometry interference analysis of radar network performance," *IEEE Communications Letters*, vol. 22, no. 11, pp. 2362–2365, 2018.
- [8] Z. Fang *et al.*, "Stochastic geometry for automotive radar interference with RCS characteristics," *IEEE Wireless Communications Letters*, vol. 9, no. 11, pp. 1817–1820, 2020.
- [9] G. Ghatak *et al.*, "A Fine-Grained Analysis of Radar Detection in Vehicular Networks," in *2021 IEEE Global Communications Conference (GLOBECOM)*. IEEE, 2021, pp. 01–06.
- [10] K. Haritha *et al.*, "Slotted aloha for FMCW radar networks," in *2021 National Conference on Communications (NCC)*. IEEE, 2021, pp. 1–6.
- [11] V. B. Sukumaran, C. Singh *et al.*, "Slotted aloha and CSMA protocols for FMCW radar networks," *arXiv preprint arXiv:2201.09030*, 2022.
- [12] S. Jin and S. Roy, "FMCW Radar Network: Multiple Access and Interference Mitigation," *IEEE Journal of Selected Topics in Signal Processing*, vol. 15, no. 4, pp. 968–979, 2021.
- [13] P. Chu *et al.*, "Interference characterization and power optimization for automotive radar with directional antenna," *IEEE Transactions on Vehicular Technology*, vol. 69, no. 4, pp. 3703–3716, 2020.
- [14] K. V. Mishra *et al.*, "Stochastic-geometry-Based interference modeling in automotive radars using Matern hard-core process," in *2020 IEEE Radar Conference (RadarConf20)*. IEEE, 2020, pp. 1–5.
- [15] L. Kui *et al.*, "Interference analysis for automotive radar using matern hard-core point process," in *2021 IEEE/CIC International Conference on Communications in China (ICCC)*. IEEE, 2021, pp. 817–822.
- [16] M. T. Shah *et al.*, "Binomial line cox processes: Statistical characterization and applications in wireless network analysis," *IEEE Transactions on Wireless Communications*, 2024.
- [17] M. T. Shah, G. Ghatak, A. Kumar, and S. S. Ram, "Modeling and statistical characterization of large-scale automotive radar networks," *arXiv preprint arXiv:2408.13645*, 2024. [Online]. Available: <https://arxiv.org/abs/2408.13645>
- [18] Y. Nabil *et al.*, "Beamwidth design tradeoffs in radar-aided millimeter-wave cellular networks: A stochastic geometry approach," *IEEE Access*, 2024.
- [19] G. Ghatak *et al.*, "Poisson networked control systems: Statistical analysis and online learning for channel access," *22nd International Symposium on Modeling and Optimization in Mobile, Ad hoc, and Wireless Networks (WiOpt 2024) workshop RAWNET*, 2024.
- [20] G. Ghatak, A. De Domenico, and M. Coupechoux, "Small cell deployment along roads: Coverage analysis and slice-aware rat selection," *IEEE Transactions on Communications*, vol. 67, no. 8, pp. 5875–5891, 2019.
- [21] S. N. Chiu *et al.*, *Stochastic geometry and its applications*. John Wiley & Sons, 2013.
- [22] D. Shnidman, "Expanded swerling target models," *IEEE Transactions on Aerospace and Electronic Systems*, vol. 39, no. 3, pp. 1059–1069, 2003.
- [23] A. Hald, *A history of probability and statistics and their applications before 1750*. John Wiley & Sons, 2005.
- [24] M. Series, "Systems characteristics of automotive radars operating in the frequency band 76–81 ghz for intelligent transport. systems applications," *Recommendation ITU-R, M*, pp. 2057–1, 2014.
- [25] M. Boban *et al.*, "Connected roads of the future: Use cases, requirements, and design considerations for vehicle-to-everything communications," *IEEE vehicular technology magazine*, vol. 13, no. 3, pp. 110–123, 2018.
- [26] 3GPP, "Service requirements for enhanced v2x scenarios," *Technical Specification (TS) 22.186, 3rd Generation Partnership Project (3GPP)*, 2019.
- [27] J. D. Alonso *et al.*, "Lane-change decision aid system based on motion-driven vehicle tracking," *IEEE Transactions on Vehicular Technology*, vol. 57, no. 5, pp. 2736–2746, 2008.
- [28] G. Sidorenko *et al.*, "Safety of automatic emergency braking in platooning," *IEEE Transactions on Vehicular Technology*, vol. 71, no. 3, pp. 2319–2332, 2021.